Integrative Metabolic Pathway Analysis Reveals Novel Therapeutic Targets in Osteoarthritis

Authors

Beatriz Rocha, Berta Cillero-Pastor, Gert Eijkel, Valentina Calamia, Patricia Fernandez-Puente, Martin R. L. Paine, Cristina Ruiz-Romero, Ron M. A. Heeren, and Francisco J. Blanco

Correspondence

fblagar@sergas.es;
valentina.calamia@sergas.es

In Brief

A defective chondrogenic differentiation of MSC is implicated in the limited regeneration capacity of osteoarthritic cartilage. We have followed a SILAC-based proteomic strategy in combination with MALDI-MSI analysis to identify proteomic and metabolomic changes underlying MSC differentiation in OA, which could provide novel targets for therapeutic intervention. Specifically, we have described that UDP-glucuronic acid and UDP-GlcNAc synthesis pathway is affected during the chondrogenic differentiation of OA cells, which consequently may alter the production of cartilage ECM components.

Graphical Abstract

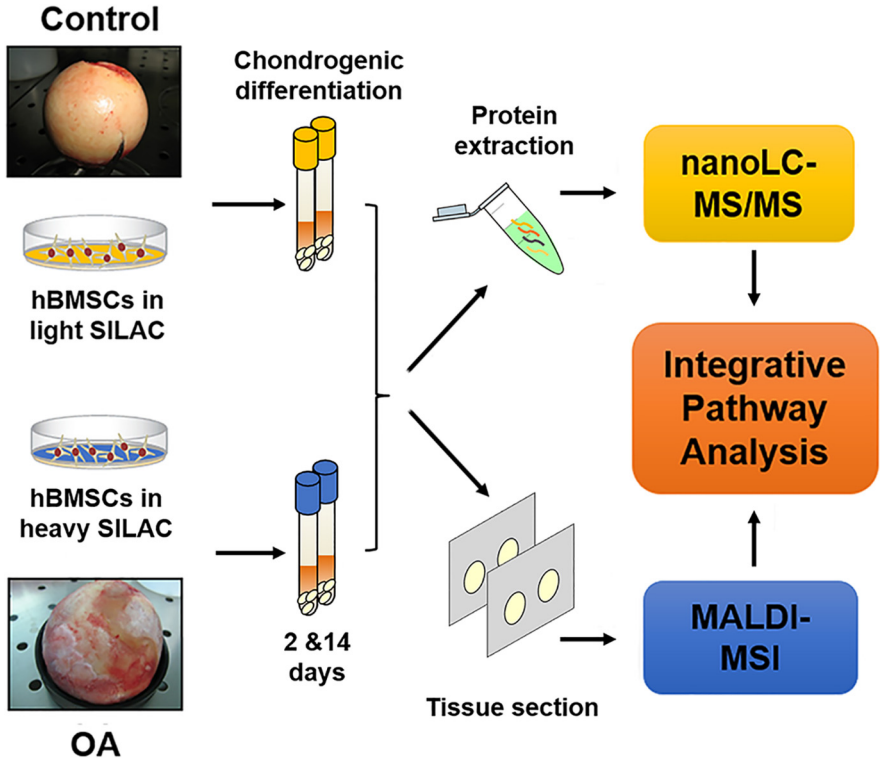

Highlights

- SILAC-based protein quantification of OA hBMSCs undergoing chondrogenesis.
- Spatially-resolved metabolomics by MSI of hBMSCs in chondrogenic differentiation.
- Differential metabolic pathways involved in OA compared to control hBMSCs.
- UDP-glucuronic acid/UDP-GlcNAc synthesis is decreased in chondrogenic OA hBMSCs.

Rocha et al., 2020, Molecular & Cellular Proteomics *19*, 574–588

https://doi.org/10.1074/mcp.RA119.001821

Integrative Metabolic Pathway Analysis Reveals Novel Therapeutic Targets in Osteoarthritis*[S]

Beatriz Rocha‡, Berta Cillero-Pastor§, Gert Eijkel§, Valentina Calamia‡‡‡, Patricia Fernandez-Puente¶, Martin R. L. Paine§, Cristina Ruiz-Romero‡, Ron M. A. Heeren§, and Francisco J. Blanco‖

In osteoarthritis (OA), impairment of cartilage regeneration can be related to a defective chondrogenic differentiation of mesenchymal stromal cells (MSCs). Therefore, understanding the proteomic- and metabolomic-associated molecular events during the chondrogenesis of MSCs could provide alternative targets for therapeutic intervention. Here, a SILAC-based proteomic analysis identified 43 proteins related with metabolic pathways whose abundance was significantly altered during the chondrogenesis of OA human bone marrow MSCs (hBMSCs). Then, the level and distribution of metabolites was analyzed in these cells and healthy controls by matrix-assisted laser desorption/ionization mass spectrometry imaging (MALDI-MSI), leading to the recognition of characteristic metabolomic profiles at the early stages of differentiation. Finally, integrative pathway analysis showed that UDP-glucuronic acid synthesis and amino sugar metabolism were downregulated in OA hBMSCs during chondrogenesis compared with healthy cells. Alterations in these metabolic pathways may disturb the production of hyaluronic acid (HA) and other relevant cartilage extracellular matrix (ECM) components. This work provides a novel integrative insight into the molecular alterations of osteoarthritic MSCs and potential therapeutic targets for OA drug development through the enhancement of chondrogenesis. ***Molecular & Cellular Proteomics 19: 574–588, 2020. DOI: 10.1074/mcp.RA119.001821.***

Articular cartilage is a connective tissue with a limited intrinsic capacity for repair, attributable to its avascular nature and low mitotic cell activity. Because of its poor healing response following injury, it is highly susceptible to osteoarthritis (OA)[1] (1). OA is currently considered a heterogeneous disease involving pathological changes in all joint tissues, including cartilage, synovium, subchondral bone, meniscus, and ligaments (2). Healthy and OA articular tissues contain mesenchymal stromal cells (MSCs) with chondrogenic capacity that may participate in the repair of cartilage lesions in OA (3, 4). Accordingly, articular tissues obtained from patients with meniscal injury and early OA are enriched in MSCs when compared with healthy (5, 6). These findings suggest that failure in articular cartilage regeneration may not be a result of limitations in the supply of MSCs but could be related to a defective chondrogenic differentiation of MSCs during attempts to restore healthy cartilage homeostasis. Drugs able to stimulate the chondrogenic capacity of MSCs in the joint represent an attractive approach for developing chondroprotective treatments or disease-modifying osteoarthritis drugs (DMOADs) (7). In this regard, it has recently been shown in a surgically-induced OA rat model that specific small molecules, when administered directly into the joint space, are able to inhibit joint destruction through Wnt signaling pathway regulation, being thus candidates for a potential disease modifying therapy for OA (8). Therefore, the elucidation of the mechanisms governing the chondrogenic differentiation of MSCs can lead to the identification of novel molecular markers that could be used as targets for alternative DMOADs development.

Proteomic approaches have been applied to increase knowledge of the differentiation processes of MSCs obtained from different tissues (9). For instance, label-free relative quantification strategies have recently been performed for the secretome and proteome characterization of hBMSCs undergoing chondrogenesis (10, 11). However, label-free proteomic methods are less accurate, less precise, and less reproducible for protein quantification compared with those based on stable isotope labeling such as stable isotope labeling by amino acids in cell culture (SILAC) (12, 13). The latter is one of

From the ‡Grupo de Investigación de Reumatología (GIR), Unidad de Proteómica, INIBIC – Complejo Hospitalario Universitario de A Coruña, SERGAS, Universidad de A Coruña, A Coruña, Spain; §The Maastricht Multimodal Molecular Imaging Institute (M4I), Division of Imaging Mass Spectrometry, Maastricht University, The Netherlands; ¶Grupo de Investigación de Reumatología, INIBIC-Complejo Hospitalario Universitario de A Coruña, SERGAS, Agrupación CICA-INIBIC, Universidad de A Coruña, A Coruña, Spain; ‖Grupo de Investigación de Reumatología, INIBIC-Complejo Hospitalario Universitario de A Coruña, SERGAS, Departamento de Medicina Universidad de A Coruña, A Coruña, Spain

Received October 11, 2019, and in revised form, January 8, 2020
Published, MCP Papers in Press, January 24, 2020, DOI 10.1074/mcp.RA119.001821

the most accurate quantitative mass spectrometry (MS) methods, because the differentially labeled samples are combined very early in the experimental workflow, which minimizes errors during sample handling (14–16). Hence, we previously applied quantitative proteomics based on SILAC to evaluate modulations in the intracellular protein profiles during chondrogenic differentiation of hBMSCs obtained from healthy donors (17).

In addition to protein expression, metabolic pathway alterations have also been associated with the modulation of chondrogenesis. Glycolysis, mitochondrial respiration, and uronic acid pathways have recently been reported to be involved in adenine triphosphate (ATP) oscillations, which play an essential role in prechondrogenic condensation (18). Other studies have also detected changes in fatty acid synthesis and amino acid production during chondrogenic differentiation of 3D-cultured hBMSCs in alginate beads using ^{1}H nuclear magnetic resonance spectroscopy (19). Thus, the global analysis of metabolic changes during chondrogenesis might also provide important information about the molecular mechanisms and potential markers of this process.

For that reason, we previously identified and visualized by matrix-assisted laser desorption/ionization-mass spectrometry imaging (MALDI-MSI) different lipid species in micromasses (3D cell aggregate systems) obtained from hBMSCs undergoing chondrogenesis (20). Although our preceding studies offered important insights about chondrogenesis in healthy circumstances, the proteomic and metabolomic analysis of hBMSCs from OA patients will increase our understanding of cartilage formation processes under pathological conditions. This can aid to identify new molecular mechanisms and targets for therapeutic interventions. Here, we evaluated the characteristic proteomic and metabolomic changes of OA hBMSCs in a chondrogenic model. Using SILAC-MS, we found statistically significant alterations in 43 proteins during the chondrogenesis of hBMSCs obtained from OA patients. The analysis of metabolic changes studied by MALDI-MSI revealed substantial differences between OA and healthy hBMSCs before and after the early stages of differentiation, specifically implicating an altered pentose/glucuronic pathway in OA. This knowledge may be instrumental for developing future therapies.

[1] The abbreviations used are: OA, osteoarthritis; AGG, agreccan; CH_6S, chondroitin-6-sulfate; COL1A1, collagen alpha-1 (I) chain; COL2A1, collagen alpha-1 (II) chain; COL10A1, collagen alpha-1 (X) chain; DA, discriminant analysis; DMOADs, disease-modifying osteoarthritis drugs; ECM, extracellular matrix; GAGs, glycosaminoglycans; HA, hyaluronic acid; hBMSCs, human bone marrow mesenchymal stromal cells; IHC, immunohistochemistry; KS, keratan sulfate; MSI, mass spectrometry imaging; PCA, principal component analysis; PGs, proteoglycans; SILAC, stable isotope labeling by amino acids in cell culture; UGDH, UDP-glucose 6-dehydrogenase; UGP2, UTP-glucose-1-phosphate uridylyltransferase.

EXPERIMENTAL PROCEDURES

Experimental Design and Statistical Rationale—The experimental design and statistical rationale for each of the proteomic and MALDI-MSI experiments conducted in this work will be described more in detail in each subsection. The discovery phase of the proteomics study was performed on three different OA biological samples without technical replication. MALDI-MSI analysis was performed on three control and five different OA samples, with two technical replicates per condition.

Human Bone Marrow Specimens—Bone marrow samples were obtained as trabecular bone biopsy specimens from femoral heads of OA patients ($n = 13$) undergoing total hip replacement surgery, and donors with no history of joint disease (control, $n = 11$). All tissue samples were provided by the Tissue Bank and the Autopsy Service at Hospital Universitario de A Coruña. OA patients were diagnosed following the criteria determined by the American College of Rheumatology (21). Informed consent was obtained from the patients before surgery. The study was approved by the local Ethics Committee (Galicia, Spain). Patient data collection including demographic and clinical characteristics (age, weight, body mass index, etc.) are summarized in supplemental Table S1.

Cell Labeling and Chondrogenic Differentiation—hBMSCs were isolated and labeled as previously described (22). hBMSCs were firstly characterized based on their negativity for CD34 and CD45 and their positivity for CD73, CD90, CD105, and CD166 by flow cytometry and their differentiation potential toward cartilage, bone and adipose tissue (23, 24). Briefly, 5×10^4 cells were seeded in Dulbecco's modified Eagle's medium (DMEM) 4.5 g/L glucose deficient in arginine and lysine, supplemented with 10% dialyzed FBS, 2 mM L glutamine, and antibiotics, containing also 28 mg/L L-arginine-HCl-$^{13}C_6{}^{15}N^4$ (Arg10) and 146 mg/L L-lysine-HCl-$^{13}C_6$ (Lys6) or the standard forms L-arginine HCl-$^{12}C_6{}^{14}N_4$ and L-lysine-HCl-$^{12}C_6$ (Lys0) (all from Silantes, Munich, Germany). Cells were subcultured every week until achieving 100% labeling. Cell viability and normal growth rates were assessed in the SILAC media supplemented with the different isotopes using a CellTiter 96® AQueous Non-Radioactive Cell Proliferation Assay (Promega, Madison, Wisconsin) kit.

SILAC-labeled cells populations were then cultured in 3D high-density pellet mass cultures or micromasses with chondrogenic differentiation medium containing 10 ng/ml TGF-β_3 for 14 days. The micromass *in vitro* culture system employed to direct stem cell differentiation into the chondrogenic lineage has been extensively stardardized and characterized in our laboratory, maintaining cell viability and the synthesis of the extracellular matrix components under our experimental conditions (23–25).

Micromasses were collected after 2 days and 14 days in culture and stored at −80 °C until further analysis. hBMSCs employed in the proteomic analysis were obtained from femoral heads of three OA patients. For MALDI-imaging experiments, micromasses were embedded in 10% gelatin at 37 °C and immediately frozen at −80 °C. For these imaging experiments, samples from five additional OA patients and three individuals with no history of joint disease were included. Additionally, gene expression assays were carried out using OA and control hBMSCs from independent experiments, five and eight, respectively.

Immunohistochemical Analyses of Cell Differentiation—For chondrogenesis evaluation, micromass pellets were frozen in OCT embedding matrix (BDH Chemicals, Poole, UK) and cut at 4 μm with a cryostat (Leica Microsystems, Barcelona, SP) for immunohistochemical evaluation. Sections were immunostained with monoclonal antibodies against aggrecan (1:100, Abcam, Cambridge, UK), chondroitin-6-sulfate (1:500, Abnova GmbH, Germany), keratan sulfate (1:100, Santa Cruz Biotechology), type II (1:200, Abcam), type I (1:1000, Abcam) and type X collagens (Sigma Aldrich, St. Louis, MO). The

peroxidase/DAB ChemMate™ DAKO EnVision™ detection kit (Dako, Barcelona, Spain) was used. Setions were counterstained with hematoxilyn and mounted with Eukitt resin. The percentage of positivity of each inmunohistochemical assay was measured using ImageJ software (NIH, Bethesda, MD). Three representative images were selected for each donor (control, $n = 5$ and OA, $n = 4$) and used for relative quantification.

Sample Preparation for MALDI-MSI—Micromass sections (10 μm) were obtained using a cryostat, mounted onto indium tin oxide (ITO), high conductivity slides (Delta Technologies, Stillwater, MN) and stored at −80 °C until further analysis. Before matrix application, slides were placed in a vacuum desiccator at room temperature and defrosted for 20 min. A matrix solution of 10 mg/ml of 9-aminoacridine (9-AA) (Sigma-Aldrich, Zwijndrecht, The Netherlands) dissolved in 70% ethanol was prepared. The matrix was then deposited onto the tissue section surface using a HTX TM-Sprayer (HTX Technologies, LLC, North Carolina). The complete loop of the sprayer (5 ml) was first flushed with the matrix solution and then applied to the sample surface. The matrix flow rate of the pump was 120 μl/min, the air pressure was set to 10 psi and a block temperature of 85 °C was chosen. The stage of the spraying device was moved at a speed of 1200 mm/min and the distance between the spray nozzle to the glass slide was set to 40 mm. Four layers of matrix were applied with 30 s of drying time between each pass to achieve homogeneous matrix coverage. In addition, the spray pattern was changed by an angle of 90° and adjusted with a line spacing of 3 mm.

Protein Extraction and In-gel Digestion—Proteins were extracted from the micromasses using a combination of a mix miller and a lysis buffer containing 6 M urea, 2 M thiourea, 4% CHAPS, 30 mM Tris-base, as previously described (17). Total protein concentrations were determined using the Bradford assay (Sigma). Heavy (micromasses at day 14) and light (micromasses at day 2) samples were then mixed in a 1:1 ratio according to the measured protein concentrations, and 15 μg of each mixed sample was resolved onto a 10% SDS-PAGE. The gel was stained with Coomassie blue, and 10 gel bands were excised. The gel pieces were washed with 50% acetonitrile (ACN) in a 25 mM ammonium bicarbonate solution until completely destained. Samples were then reduced with 10 mM dithiothreitol for 30 min at 56 °C and alkylated with 54 mM iodoacetamide for 10 min in the dark. Digestion was performed overnight with 6.66 ng/μl sequencing-grade modified trypsin (Promega) at 37 °C. Trifluoroacetic acid (TFA) (1% final concentration) was added to the peptide mixtures to stop the enzymatic reaction. Peptides were then extracted from the gel pieces with 50% ACN/0,1% TFA. Extracted peptide mixtures were desalted and concentrated employing NuTips (Glygen, Columbia, MD), dried in a speedvac and stored at −80 °C until LC-MS/MS analysis.

Mass Spectrometry Analysis—The peptide fractions were separated using reversed phase chromatography in a nanoLC system (Tempo, Eksigent, Dublin, CA) by loading through a trap column into a C18 silica-based column (Integrafit C18, ProteopepTM II, 75 μm id, 10.2 cm, 5 μm, 300 Å, New Objective, Woburn, MA). Peptides were eluted at a flow rate of 350 nl/min during a 120-min linear gradient from 5 to 45% B (mobile phase B: 0.1% TFA 80% ACN), mixed with α-cyano-4-hydroxycinnamic acid matrix (3 mg/ml at a flow rate of 1.2 μl/min) and deposited onto a MALDI plate using an automatic spotter (SunCollect, Sunchrome, Friedrichsdorf, Germany).

Data acquisition was carried out using a 4800 MALDI-TOF/TOF instrument (AB Sciex, Foster City, CA) with a 200-Hz repetition rate (Nd/YAG laser). MS full-scan spectra from 800 to 4000 *m/z* were acquired for each peptide-containing LC spots using 1500 laser shots and a laser intensity of 3800 kV. After screening of all LC-MALDI sample positions in MS positive reflector mode, the fragmentation of automatically selected precursors was performed at a collision energy of 1 kV with a collision-induced dissociation (CID) gas (air). Up to 12 of the most intense ion signals per spot position with signal/noise ratio (S/N) above 80 were selected as precursors for tandem mass spectrometry (MS/MS) analysis, excluding common trypsin autolysis peaks and matrix peaks. The number of shots was 1800 for MS/MS, and the laser intensity was set to 4700 kV. A second MS/MS was performed, excluding the precursors selected in the previous MS/MS run. Precursors with S/N >30 were selected to identify proteins that were not identified in the first MS/MS analysis.

Proteomic Data Analysis—Proteomic data analysis was performed on three different OA biological replicates without technical replication. Data was acquired using 4000 Series Explorer v.3.7. Protein identification and quantification were carried out using ProteinPilot™ software v.4.0 (AB Sciex). Each MS/MS spectrum was searched in the Uniprot/Swissprot database (UniProt 2015_05 release version containing 547,599 sequences and 195,014,757 residues, with taxonomy restriction_Homo sapiens) using the Paragon Algorithm. The following ProteinPilot search parameters were used: sample type set as SILAC (Lys +6, Arg+10), oxidation of methionine residue as variable modification, iodoacetamide alkylation of cysteine residue as a fixed modification and a maximum of one missed cleavage allowed for trypsin. The ProteinPilot software also calculated a confidence percentage, the Unused score, which reflects the probability of a hit being a false positive. Data were also normalized for loading error by bias correction. Searches against a concatenated database containing both forward and reversed sequences allowed the false discovery rate to be kept at 1%. Common contaminants such as trypsin autolysis peaks and matrix ion signals were excluded from the analysis. The theoretical ions and the peaks were matched using the same tolerance used by the Paragon Algorithm search. The tolerance used for matching is based on information about the mass accuracy of the instrument chosen in the Paragon Method dialog box. We considered statistically significant only those changes with a p value <0.05 and ±20% change in expression from day 2 to day 14. GO enrichment analysis on the set of modulated proteins was performed using Uniprot database.

MALDI-FT-ICR-MSI Experiments—Sprayed tissue sections were optically scanned and imported into FlexImaging 4.1 software (Bruker Daltonik GmbH, Bremen, Germany) to define the area of the sample to be imaged. Tissue sections were then analyzed using a Bruker 9.4 T solariX FT-ICR mass spectrometer equipped with a SmartBeam II Nd:YAG laser operated with the MALDI source. Samples from each donor were analyzed in duplicate. The instrument external calibration was performed using a solution of red phosphorous (Sigma) ranging between mass/charge (*m/z*) 50–1000 Da before MALDI-FT-ICR-MSI analysis. The analytical parameters for the on-line calibration were as follows: mode, linear; threshold (abs), 1×10^5; mass tolerance, 10 ppm; reference masses *m/z* 193.07602 (9-AA), *m/z* 346.05471 (AMP), *m/z* 426.02104 (ADP) and *m/z* 505.98737 (ATP). Data were acquired at a spatial resolution of 30 μm using FlexControl software. Each mass spectrum was obtained from a single scan of 200 laser shots using 1 million data points in negative ionization mode within a mass range of *m/z* 100–1000 Da, a laser power of 22% and a frequency of 2000 Hz. MALDI-MSI images of differentially expressed metabolites were generated with FlexImaging 4.1 software (Bruker Daltonik GmbH). These images were also obtained with a mass window of ± 0.001 Da and normalized using root means square (RMS). Following MSI analysis, the slides were rinsed in 70% ethanol to remove the matrix. Then, the slides were subsequently stained with hematoxylin and eosin (H&E). Optical images of all stained tissue sections were acquired using a MIRAX desk scanner (Zeiss, Gottingen, Germany) to spatially co-relate the ion distribution to histology.

Multivariate Statistical Analysis of MALDI-FT-ICR-MSI Data—Principal component analysis (PCA) and discriminant analysis (DA) were employed to look for spectral similarities and differences between the

samples collected at day 2 and 14, using an in-house built ChemoneTricks toolbox for MATLAB version 2014A (The MathWorks, Natick, MA). The MS raw data were first converted to the MATLAB format. Then, all the spectra generated in the MSI experiments from the two time points of all OA and control donors were combined and peak-picked before PCA. Peak picking was performed with the in-house-built PEAPI software to reduce the data set to a size that enables the computational methods needed (26). The number of principal components used as input for DA was limited to one quarter of the total number spectra to prevent overfitting of the DA model. PCA-DA was applied independently to the biological and technical replicates to evaluate the reproducibility among donors. After data analysis, *m/z* values were selected for further identification. Metabolites with DF1 score loadings $>\pm 5$ according to PCA-DA analysis, and a *p* value <0.05 by the Mann-Whitney test were considered significantly altered.

Metabolite Identification by Tandem Mass Spectrometry—Tandem mass spectrometry (MS/MS) was performed using CID in an ion trap mass analyzer from the MALDI-LTQ-Orbitrap Elite mass spectrometer directly on the micromass sections using a collision energy of 38 and an isolation width of 0.7 Da. Data were analyzed using Xcalibur software 2.3.26 (Thermo Fisher Scientific, Bremen, Germany). Identifications were based on the high mass accuracy and resolution of the precursor mass and MS/MS analyses compared with metabolite and lipid databases, such as the Human Metabolome Database (HMDB) http://www.hmdb.ca (27), METLIN (http://metlin.scripps.edu) (28) and LipidMaps (www.lipidmaps.org) (29). For the assignments, 5 ppm mass accuracy was selected as the tolerance window. If MS/MS spectra were not available in the databases or did not match with the expected theoretical spectra, metabolites matching the precursor mass in either HMBD, METLIN or LipidMaps were subjected to manual interpretations to attempt to match experimental MS/MS spectra with expected fragment structures. Metabolite assignments, with their corresponding mass errors and MS/MS structural validation, are summarized in supplemental Table S2. As an example, we assigned the peak at *m/z* 540.0474 to the $[M\text{-}H_2O\text{-}H]^-$ ion of adenine diphosphate (ADP)-ribose based on the accurate mass difference (1.1 ppm) and the interpretation of the MS/MS spectrum following collision-induced dissociation of ions at *m/z* 540.0533 (supplemental Fig. S1).

Enrichment, Pathway and Integrative Metabolic Analysis—The differentially expressed metabolites from the comparative analyses of OA *versus* control and day 2 *versus* day 14 were further subjected to enrichment and pathway analysis using MetaboAnalyst software 4.0 (30). Pathway analysis combines the results obtained from enrichment and topology analysis to visualize the most relevant metabolic processes involved in the studied conditions. MetaboAnalyst is based on different databases, including the Kyoto encyclopedia of genes and genomes (KEGG) (31), small molecule pathway database (SMPD) (32) and HMBD for the identification of relevant metabolic pathways. Finally, we performed an integrated analysis combining metabolomic and protein expression studies. In this analysis, both metabolites and genes/proteins were mapped to KEGG metabolic pathways for over-representation analysis (ORA) and topology analysis. Topology analysis uses the structure of a given pathway to evaluate the relative importance of the matched proteins/metabolites based on their relative location. The algorithms used for ORA and topology analysis were the hypergenometric test and betweenness centrality, respectively. Pathway significance is determined from enrichment analysis and the impact value is based on topology analysis. Pathways were considered significant when the *p* value calculated from the enrichment analysis were ≤ 0.05.

RNA Extraction and Quantitative Real-time PCR Assays—Total RNA was isolated using Trizol Reagent (Invitrogen, Carlsbad, CA), according to the manufacturer's instructions. After RNA extraction, 1 μg of RNA was reverse transcribed into complementary DNA (cDNA) using SuperScript™ VILO™ cDNA synthesis kit in accordance with the manufacturer's instructions and was analyzed by quantitative real-time PCR (qRT-PCR). The reactions were carried out in 96-well plates in duplicate using a LightCycler 480-II Instrument (Roche, Mannheim, Germany) with TaqMan Universal Master Mix (Applied Biosystems, Foster City, CA). Primers for UTP-glucose-1-P-uridylyltransferase (UGP2), UDP-glucose dehydrogenase (UGDH) and Ribosomal protein L13a (RPL13a) were designed using the Universal Probe Library tool from the Roche website. Data were analyzed using Qbase+ software (Biogazelle, Gent, Belgium). Gene expression was normalized to the housekeeping gene RPL13a (selected after GeNorm expression stability assesment) and expressed as the x-fold change relative to day 2. Sequence primers, probes and PCR conditions are given in supplemental Table S3.

Statistical Analysis—A *p* value < 0.05 was considered statistically significant and statistical tests were two-sided. Data were analyzed using GraphPad Prism software 7.0. and presented in the figure legends or text as mean ± S.E. of the mean (SEM). Two-group comparisons (day 2 *versus* day 14) were carried out using the Mann-Whitney test with significant values indicated as follows: **p* value <0.05, ***p* value <0.01, ****p* value <0.001, n.s. not significant.

RESULTS

Characterization of Control and OA hBMSCs Undergoing Chondrogenic Differentiation—hBMSCs derived from normal individuals and OA patients were pelleted and cultured in a chondrogenic differentiation medium for 14 days. To confirm chondrogenic induction of hBMSCs, well-known chondrocyte markers were assessed using immunohistochemical analyses. In line with previous studies (17, 22) we observed the up-regulation of aggrecan (Agg), chondroitin-6-sulfate (CH_6S) and keratan sulfate (KS) by chondrogenic factors at day 14 compared with day 2, and these differences were statistically significant (**p* value <0.05 (Agg and KS); ****p* value <0.001 (CH_6S)), demonstrating the chondrogenic differentiation of normal hBMSCs under our culture conditions (Fig. 1*A*–1*C*). OA hBMSCs also showed statistically significant higher expression levels of CH_6S and KS at day 14 of chondrogenesis (**p* value <0.05). However, the expression levels of KS and Agg were notably lower compared with control hBMSCs at day 14 (**p* value <0.05). Immunohistochemistry (IHC) results for collagen alpha-1 (II) chain (COL2A1) were also positive at day 14 for both control and OA hBMSCs (Fig. 1*D*), although there were not statistically significant differences between the two time points assessed. Additionally, the expression of collagen alpha-1 (I) chain (COL1A1), considered as a fibrocartilage/dedifferentiated chondrocyte marker, was greatly increased in OA (**p* value <0.05) but not in control micromasses during chondrogenesis (Fig. 1*E*). Finally, the IHC analysis demonstrated the higher presence of collagen alpha-1 (X) chain (COL10A1), considered as the standard marker for chondrocyte hypertrophy, within OA cell pellets at day 14 compared with control samples (Fig. 1*F*), which indicates an early hypertrophic phenotype of OA hBMSCs compared with control cells.

Differentially Expressed Proteins During the Chondrogenesis of OA hBMSCs—To analyze and quantify protein changes occurring during chondrogenesis, undifferentiated (day 2) and

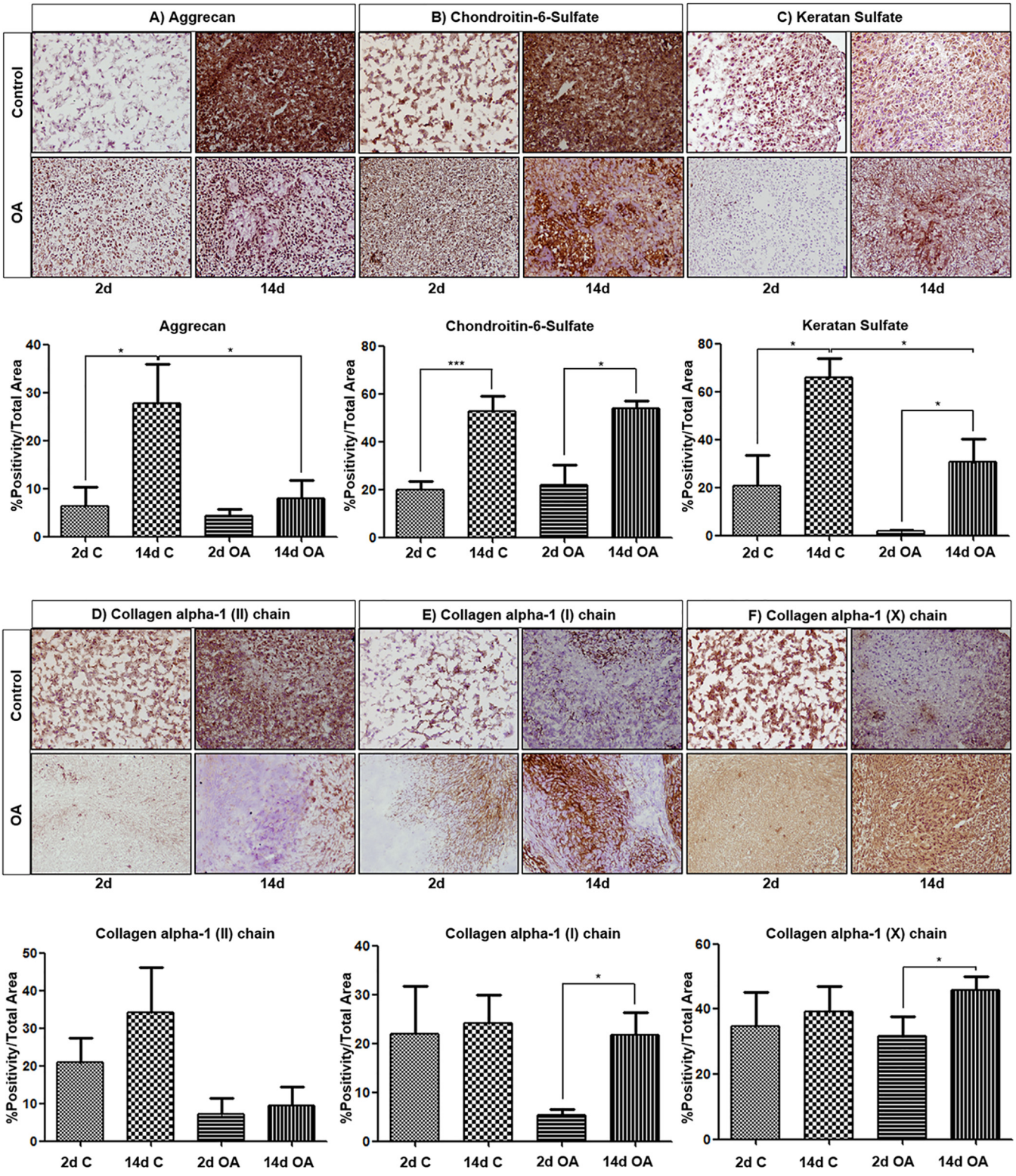

FIG. 1. **Chondrogenic differentiation of control and OA hBMSCs.** *A*, Immunodetection of aggrecan, *B*, chondroitin-6-sulfate, *C*, keratan sulfate, *D*, collagen alpha-1 (II) chain, *E*, collagen alpha-1 (I) chain and *F*, collagen alpha-1 (X) chain, assessed on control and OA micromasses after 2 and 14 days of chondrogenesis. Representative images of the inmunoanalysis (normal, $n = 4$; OA, $n = 5$) are shown in the panels (magnification x20). In (*A–F*), quantitative analysis data are presented as mean percentage positivity/total micromass area ± SEM. **p* value <0.05, ***p* value <0.01, ****p* value <0.001 (Mann Whitney test). *C*, control; OA, osteoarthritis; 2d, 2 days; 14d, 14 days.

TABLE I
Chondrogenesis-regulated proteins in OA hBMSCs, identified in this work by SILAC and nano-LC-MS/MS analysis

Acc No[a]	Protein name	Gene symbol	Pept (95%)[b]	Ratio[c]	*p* value	EF[d]
Proteins increased at day 14 of chondrogenic differentiation						
Q04446	1,4-alpha-glucan-branching enzyme	GBE1	6	2411	0.005	1,612
P21589	5′-nucleotidase	5NTD	4	1559	0.030	1438
P15121	Aldose reductase	AKR1B1	3	2779	0.046	EF > 2
P15144	Aminopeptidase N	ANPEP	20	1637	0.000	1086
P07355	Annexin A2	ANXA2	88	1458	0.000	1085
P08758	Annexin A5	ANXA5	50	1583	0.000	1096
P25705	ATP synthase subunit alpha, mitochondrial	ATPA	5	1271	0.042	1255
P06576	ATP synthase subunit beta, mitochondrial	ATPB	16	1231	0.024	1194
P98160	Basement membrane-specific heparan sulfate proteoglycan core protein or Perlecan	HSPG2	2	1940	0.030	1652
P12109	Collagen alpha-1(VI) chain	COL6A1	8	1512	0.040	1480
P12110	Collagen alpha-2(VI) chain	COL6A2	19	1921	0.000	1179
P12111	Collagen alpha-3(VI) chain	COL6A3	87	1866	0.000	1112
P14625	Endoplasmin	HSP90B1	30	1514	0.002	1272
P04406	Glyceraldehyde-3-phosphate dehydrogenase	GAPDH	62	1362	0.012	1263
P62826	GTP-binding nuclear protein Ran	RAN	4	2027	0.011	1492
Q9BTM1	Histone H2A type 1-J	H2AFJ	11	2135	0.005	1572
P62807	Histone H2B type 1-C/E/F/G/I	HIST1H2BC	23	2516	0.000	1471
P62805	Histone H4	HIST1H4A	19	2518	0.003	1688
P00338	L-lactate dehydrogenase A chain	LDHA	30	1545	0.001	1247
P07195	L-lactate dehydrogenase B chain	LDHB	7	2099	0.025	1757
P43490	Nicotinamide phosphoribosyltransferase	NAMPT	4	1501	0.033	1507
P30041	Peroxiredoxin-6	PRDX6	5	1380	0.032	1323
P00558	Phosphoglycerate kinase 1	PGK1	38	1437	0.048	1433
P18669	Phosphoglycerate mutase 1	PGAM1	14	1402	0.000	1164
P02545	Prelamin-A/C	LMNA	45	1420	0.021	1343
Q6DRA6	Putative histone H2B type 2-D	HIST2H2BD	5	3595	0.006	1539
P46940	Ras GTPase-activating-like protein	IQGA1	3	1938	0.045	1885
P04179	Superoxide dismutase [Mn], mitochondrial	SOD2	16	2040	0.002	1434
P24821	Tenascin	TNC	18	1756	0.034	1674
P29401	Transketolase	TKT	4	1706	0.043	1631
P60174	Triosephosphate isomerase	TPI1	26	1530	0.001	1264
O14773	Tripeptidyl-peptidase 1	TPP1	4	1658	0.006	1257
Q16851	UTP-glucose-1-phosphate uridylyltransferase	UGP2	2	1449	0.049	1443
Proteins decreased at day 14 of chondrogenic differentiation						
P61981	14–3-3 protein gamma	1433G	10	0.791	0.046	1254
P62277	40S ribosomal protein S13	RS13	2	0.601	0.038	1580
P13639	Elongation factor 2	EEF2	9	0.682	0.024	1374
P21333	Filamin-A	FLNA	56	0.509	0.001	1475
P13489	Ribonuclease inhibitor	RNH1	13	0.239	0.034	EF > 2
P50454	Serpin H1	SERPINH1	21	0.577	0.002	1351
Q9Y490	Talin-1	TLN1	17	0.425	0.017	1974
Q01995	Transgelin	TAGLN	15	0.171	0.000	EF > 2
P67936	Tropomyosin alpha-4 chain	TPM4	11	0.297	0.001	1480
O60701	UDP-glucose 6-dehydrogenase	UGDH	11	0.759	0.026	1255

[a]Protein accession number according to SwissProt and TrEMBL databases.
[b]Number of unique peptides (Pept) used for protein identification at 95% confidence.
[c]Average SILAC ratios ($n = 3$) that represent the relative protein abundance in hBMSCs at day 14 versus day 2 of chondrogenic differentiation.
[d]Error factor (a measure of the error in the average ratio), calculated by Protein Pilot 4.0 software for quantification accuracy.
MS = mass spectrometry; LC = liquid-chromatography; SILAC = stable isotope labelling by amino acids in cell culture; OA hBMSCs = osteoarthritic human bone marrow mesenchymal stem cells.

differentiated (day 14) hBMSCs obtained from OA patients ($n = 3$) were compared using SILAC-MS. The experimental workflow (supplemental Fig. S2) for the proteomic profiling of chondrogenic-induced hBMSCs led to the identification of 281 proteins (supplemental Table S4), of which 43 proteins displayed statistically significant (±20% change; p value < 0.05) quantitative differences between the two stages of chondrogenesis (Table I). Detailed information of the identified proteins, with their corresponding peptides, is shown in supplemental Table S5.

From these 43 proteins, 33 were significantly increased and 10 were significantly decreased. The up-regulated proteins include several typical structural proteins of the cartilage ECM, including perlecan (33), the three alpha chains of type VI collagen (34) or tenascin (35), and also many different glycolytic enzymes, such as glyceraldehyde-3-phosphate dehydrogenase (GAPDH), phosphoglycerate kinase 1 (PGK1), and triosephosphate isomerase (TPI1). The downregulated proteins included cytoskeleton-related proteins, such as tropomyosin alpha-4 chain (TPM4), talin-1 (TLN1), and transgelin (TAGLN).

To further elucidate the molecular mechanisms and related biological functions involved in chondrogenic differentiation of OA hBMSCs, we classified the set of 43 differentially abundant proteins according to their biological process using the Gene Ontology (GO) database (supplemental Fig. S3). The 33 proteins increased at the advanced stage of differentatiton (day 14) are involved in three main GO biological processes: (A) metabolism, including glycolysis (GAPDH, PGAM1, PGK1, TPI1, LDHA), glucuronate interconversion (AKR1B1, UGDH, UGP2), and the pentose phosphate pathway (TKT); (B) ECM organization (ANXA2, COL6A1, COL6A2, COL6A3, TNC); and (C) regulation of transcription (H2AFJ, HIST1H2BC, HIST1H4A). Inversely, proteins decreased at day 14 are mainly related with (A) cytoskeleton reorganization (TLN1, TPM4, TAGLN); (B) regulation of transcription (RNH1); and (C) protein synthesis, folding and transport (EEF2, SERPINH1).

Metabolic Changes in OA Chondrogenesis Compared With Healthy Controls—Because more than 45% of the differentially abundant proteins quantified by SILAC are involved in glycolysis and other metabolic processes, we then investigated the metabolic profile of OA hBMSCs undergoing chondrogenesis and compared it to cells from healthy donors as controls. The metabolite levels and distribution were analyzed by MALDI-Fourier transform-ion cyclotron resonance-MSI in cryosections of control ($n = 3$) and OA ($n = 5$) micromasses at day 2 (undifferentiated) and day 14 (early differentiated stage).

Combined multivariate statistical analysis—in particular principal component analysis (PCA) and discriminant analysis (DA)—were performed on the resulting spectra that were acquired in the *m/z* range 100–1000 Da and applied independently to controls and OA samples. These analyses revealed that the metabolic profile of micromasses collected at day 2 is markedly distinct from that of micromasses at day 14 in both control (Fig. 2*A*–2*B*) and OA conditions (Fig. 2*C*–2*D*). Initially, we observed that healthy and diseased cells exhibited a similar metabolic profile at day 2, presenting a higher abundance of nucleotides such as UMP, UDP and UDP-*N*-Acetyl-glucosamine (UDP-GlcNAc). However, they exhibited marked metabolic differences at day 14. For instance, increased levels of the sugar phosphate dihydroxyacetone phosphate (DHAP) and cholesterol sulfate were specific to healthy chondrocyte-like cells (Fig. 2*B*, positive loadings), whereas several sugar nucleotides such as ADP-ribose and UDP-glucose, as well as fatty acids such as oleic acid, stearic acid and arachidonic acid, were specific to OA chondrocyte-like cells at 14 days of chondrogenic differentiation (Fig. 2*D*, positive loadings, supplemental Table S2). We identified 35 metabolites in OA samples that showed significant discrimination between days 2 and 14 (Fig. 3, $p < 0.05$). Finally, to determine which metabolites were specific to healthy and OA hBMSCs during chondrogenic differentiation, a multivariate statistical analysis was then applied to all samples (Fig. 2*E*–2*F*). As illustrated in the frequency plot of Fig. 2*E*, the second discriminant function (DF2) showed a clear difference between control and OA samples according to their metabolic composition. Based on their loadings, the metabolites discriminating between control and OA were mainly nucleotides, sugar species and phosphatidic acid-related molecules (Fig. 2*F*). On the one hand, the metabolic profile of the control samples (Fig. 2*F*, positive loadings) included several PA-related metabolites, such as the lysophosphatidic acid LPA(18:0), the cyclic phosphatidic acids cPA(18:1) and cPA(18:0), and the phosphatidic acids PA(16:1_18:0), PA(18:0_18:2) and PA(18:0_18:1). On the other hand, the characteristic OA metabolic profile confirmed an abundance of nucleotides including ADP, UMP and UDP; several fatty acids such as oleic and stearic acid; certain sugar species, such as glucose monophosphate, *N*-Acetyl-glucosamine-phosphate (GlcNAc-P), ADP-ribose and UDP-GlcNAc; and specific phospholipids such as phosphatidylinositol (PI) and phosphatidylglycerol (PG) species (Fig. 2*F*, negative loadings).

Pathway Analysis Shows Alterations of Five Differential Metabolic Processes in OA hBMSCs Compared With Controls—Using MetaboAnalyst software, the functional role of these metabolites was determined by pathway analysis (Fig. 4*A* and 4*B*). All metabolic pathways that were identified for control and OA samples are provided in supplemental Table S6 and supplemental Table S7. In both control and OA samples, purine and pyrimidine metabolism pathways were significantly altered during chondrogenesis (Fig. 4*A* and 4*B*; $p < 0.003$). Five additional metabolic pathways were significantly modulated specifically in OA samples (Fig. 4*B*; $p < 0.05$), which included galactose metabolism, amino sugar and nucleotide sugar metabolism, starch and sucrose metabolism, glycolysis or gluconeogenesis, and glycerolipid metabolism.

To further elucidate the metabolic pathways involved in normal and OA hBMSCs undergoing chondrogenic differentiation, we also performed an integrative pathway analysis using the datasets from the significantly modulated proteins and metabolites. This analysis took into account the total number of metabolites/proteins that match with a particular pathway (enrichment analysis) and the structure of the network, considering the position of the molecules inside the pathway (topology analysis). For the control pathway analysis, we integrated 17 metabolites (supplemental Fig. S4) with 51 known proteins that had shown statistically significant quantitative alterations in control hBMSCs undergoing chondro-

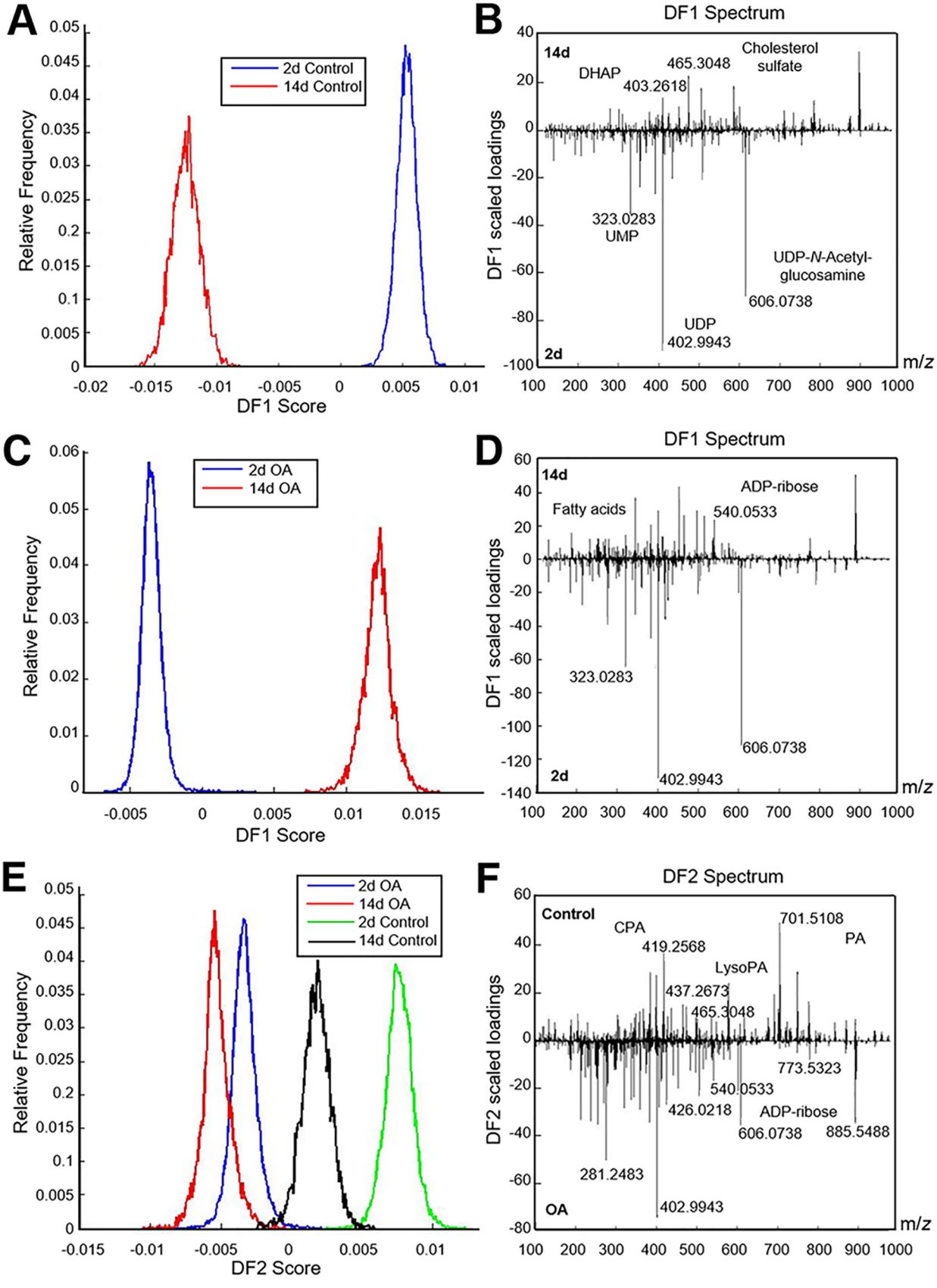
A
Relative Frequency
DF1 Score
2d Control
14d Control
B
DF1 Spectrum
DF1 scaled loadings
14d
DHAP
403.2618
465.3048
Cholesterol sulfate
323.0283
UMP
UDP-N-Acetyl-glucosamine
606.0738
UDP
402.9943
2d
m/z
C
Relative Frequency
DF1 Score
2d OA
14d OA
D
DF1 Spectrum
DF1 scaled loadings
14d
Fatty acids
ADP-ribose
540.0533
323.0283
606.0738
402.9943
2d
m/z
E
Relative Frequency
DF2 Score
2d OA
14d OA
2d Control
14d Control
F
DF2 Spectrum
DF2 scaled loadings
Control
CPA
419.2568
701.5108
PA
LysoPA
437.2673
465.3048
773.5323
540.0533
426.0218
ADP-ribose
606.0738
885.5488
281.2483
OA
402.9943
m/z

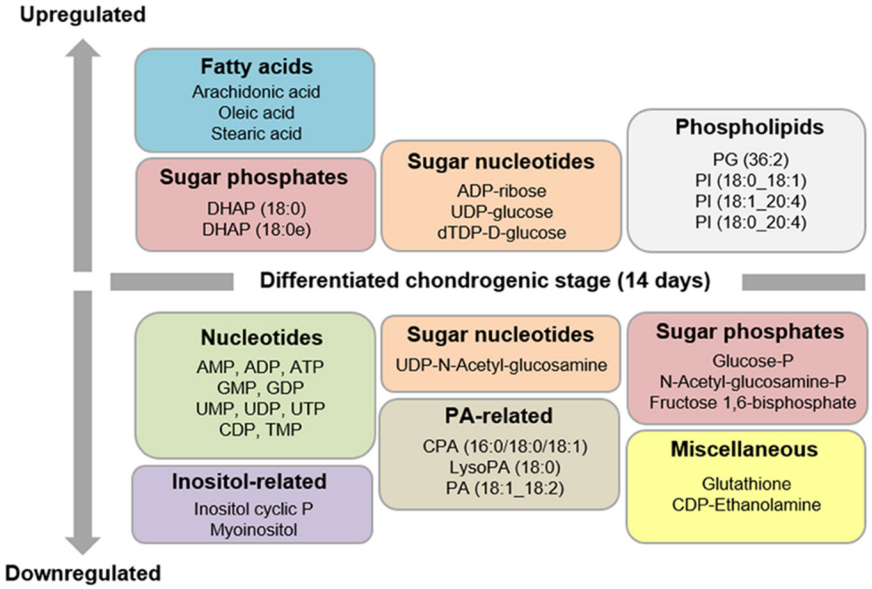

FIG. 3. **Metabolites altered in OA hBMSCs because of the chondrogenic differentiation process.** Levels of 35 metabolites, including phospholipids, were significantly altered (p value <0.05) at day 14 when compared with day 2 of chondrogenic differentiation. DHAP, dyhidroxyacetone phosphate; PA, phosphatidic acid; CPA, cyclic phosphatidic acid; LysoPA, lysophosphatidic acid; P, phosphate; PG, phosphatidylglycerol; PI, phosphatidylinositol.

genesis (17). In the analysis of OA samples, we combined 35 metabolites (Fig. 3) with the 43 proteins significantly modulated in OA hBMSCs between the two time points of chondrogenesis (Table I). The glycolysis pathway was statistically significant (p value < 0.004) in both control (Fig. 4*C*) and OA (Fig. 4*D*) samples. Other pathways involved in the chondrogenic differentiation of healthy cells were galactose metabolism and fructose/mannose metabolism, but they were not significant (supplemental Table S8). In contrast, five pathways were significantly altered (p value $= 0.05$) in OA hBMSCs undergoing chondrogenesis: pentose and glucuronate interconversions; galactose, starch, and sucrose metabolism; amino sugar and nucleotide sugar metabolism; and biosynthesis of unsaturated fatty acids (Fig. 4*D* and supplemental Table S9).

Alteration of the Glucuronic Acid Synthesis Pathway in OA hBMSCs Undergoing Chondrogenesis—Given our finding that pentose and glucuronate interconversion (KEGG pathway map00040) is one of the main altered metabolic pathways during the chondrogenesis of OA hBMSCs (Fig. 4*D*), we investigated the correspondent substrates by MALDI-MSI. The main findings of this analysis are illustrated in Fig. 5. In this pathway, UDP-glucose - a key intermediate in the formation of UDP-glucuronic acid - is synthesized from glucose monophosphate (GP) and UTP in a reaction catalyzed by UTP-glucose-1-phosphate uridylyltransferase (UGP2). Our proteomics data (Table I) showed a significant increase in UGP2 (p value < 0.05) at day 14 compared with day 2, which correlates with reductions in levels of glucose monophosphate (Fig. 5*A*) and UTP. UDP-glucose is then oxidized by UDP-glucose 6-dehydrogenase (UGDH) to generate UDP-glucuronic acid (Fig. 5*B*). Remarkably, we observed in the proteomic analysis a significant reduction in UGDH day 14 compared with day 2 (Table I, p value < 0.03), which may contribute to the significant accumulation of UDP-glucose at day 14 that can be detected in the micromass core at day 14 (Fig. 5*B*). Although UGP2 was significantly increased at the protein but not the mRNA level (Fig. 5*F*), we did detect a significant down-regulation of UGDH at day 14 specifically in OA hBMSCs (Fig. 5*G*, p value ≤ 0.05). Also within this pathway, GlcNAc-P is derived from glucose monophosphate and converted to UDP-GlcNAc. Both GlcNAc-P and UPD-GlcNAc levels were decreased in the micromasses collected at day 14 compared with day 2 (Fig. 5*D*–5*E*). This indicates a down-regulation of the amino sugar nucleotide metabolism during the chondrogenic differentiation of OA hBMSCs. Altogether, these data suggest a reduction in the synthesis of UDP-glucuronic acid and UDP-GlcNAc during the chondrogenic differentiation of OA cells that could affect HA synthesis and, as a consequence, the production of other key glycosaminoglycans (GAGs) and proteoglycans (PGs) from the cartilage ECM.

A comparison of metabolite ion maps and the H&E stainings highlighted the distinct regional distribution of glucose monophosphate. We observed that OA micromasses collected at day 2 presented higher levels of glucose monophos-

FIG. 2. **Control and OA hBMSCs undergoing chondrogenesis exhibit distinct metabolomic features.** *A*, *B*, *E*, Histogram score plots of the PCA-DA analysis based on metabolomic profiles and discriminating between days 2 and 14 of control hBMSCs (*A*), days 2 and 14 of OA hBMSCs (*B*), control and OA hBMSCs (*E*) undergoing chondrogenic differentiation. *B*, *D*, Discriminant fuction 1 (DF1) spectra loading plots showing the discriminating masses between days 2 and 14 of control hBMSCs (*B*) and days 2 and 14 of OA hBMSCs (*D*) undergoing chondrogenic differentiation. *F*, Discriminant fuction 2 (DF2) spectra loading plot showing the discriminating masses between control (days 2 and 14) *versus* OA micromasses (days 2 and 14).

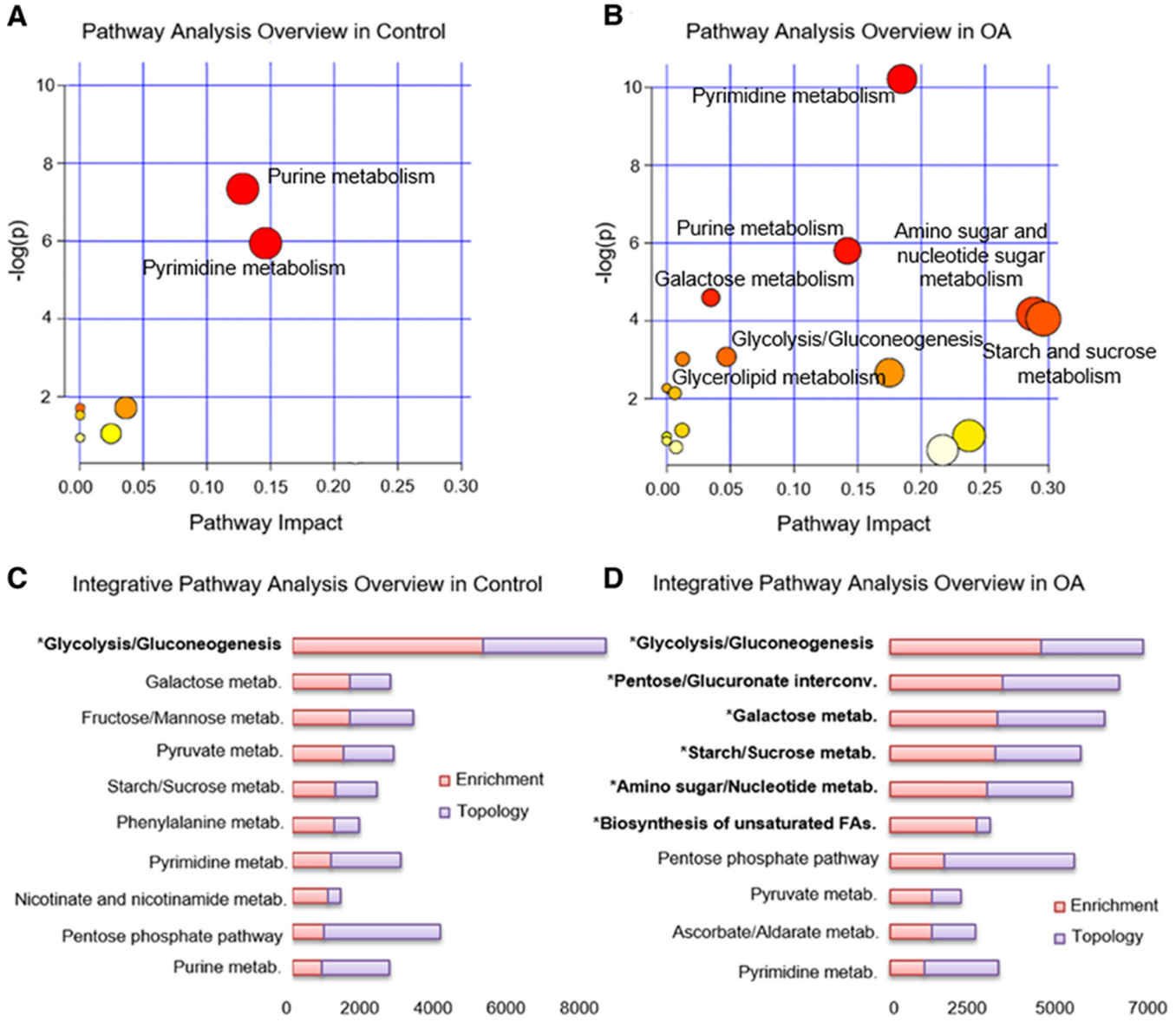

FIG. 4. **Metabolic and integrative pathway analysis overview observed in hBMSCs during chondrogenesis.** *A*, *B*, Metabolic pathways significantly altered in control (*A*) and OA (*B*) hBMSCs between day 2 and day 14 of chondrogenesis. *C*, *D*, Top 10 altered pathways observed by integrative pathway analysis for control (*C*) and OA (*D*) hBMSCs during chondrogenesis. All the matched pathways identified based on overrepresentation analysis (ORA) are visualized by circles, with the circle size indicating pathway impact (arbitrary scale). The color of the circles indicates unadjusted *p* values (*y* axis) from pathway enrichment analysis, with red < 0.003; orange < 0.2, and yellow < 0.4 for panel A and, red < 0.02; orange < 0.1, and yellow < 0.5 for panel B. The *x* axis represents increasing metabolic pathway impact according to the degree of centrality from topology analysis. Terms highlighted with an asterisk were significantly altered (*p* value < 0.05).

phate in the micromass core, whereas this metabolite showed a higher abundance in the surrounding cells of the micromass at day 14 (Fig. 5*A*). Another glycolytic intermediary metabolite, such as DHAP, was also mainly distributed in the cells of the micromass core at day 14 (supplemental Fig. S5). These findings suggest that, at day 14, the hBMSCs that are localized in the core have a higher glycolytic activity. This leads to an increased glucose consumption compared with those hBMSCs localized in the peripheral areas of the micromasses.

Undifferentiated OA hBMSCs Have an Altered Pentose Phosphate Pathway—Once observed the metabolic pathways involved during the chondrogenesis of control and OA hBMSCs, we next aimed to determine other specific metabolites potentially altered before the beginning of chondrogenesis. With this objective, we compared their metabolic profiles at the undifferentiated stage (day 2). The levels of thirty-two metabolites were distinct between OA and controls at this time point (supplemental Table S10). Among these, 10 were classified as nu-

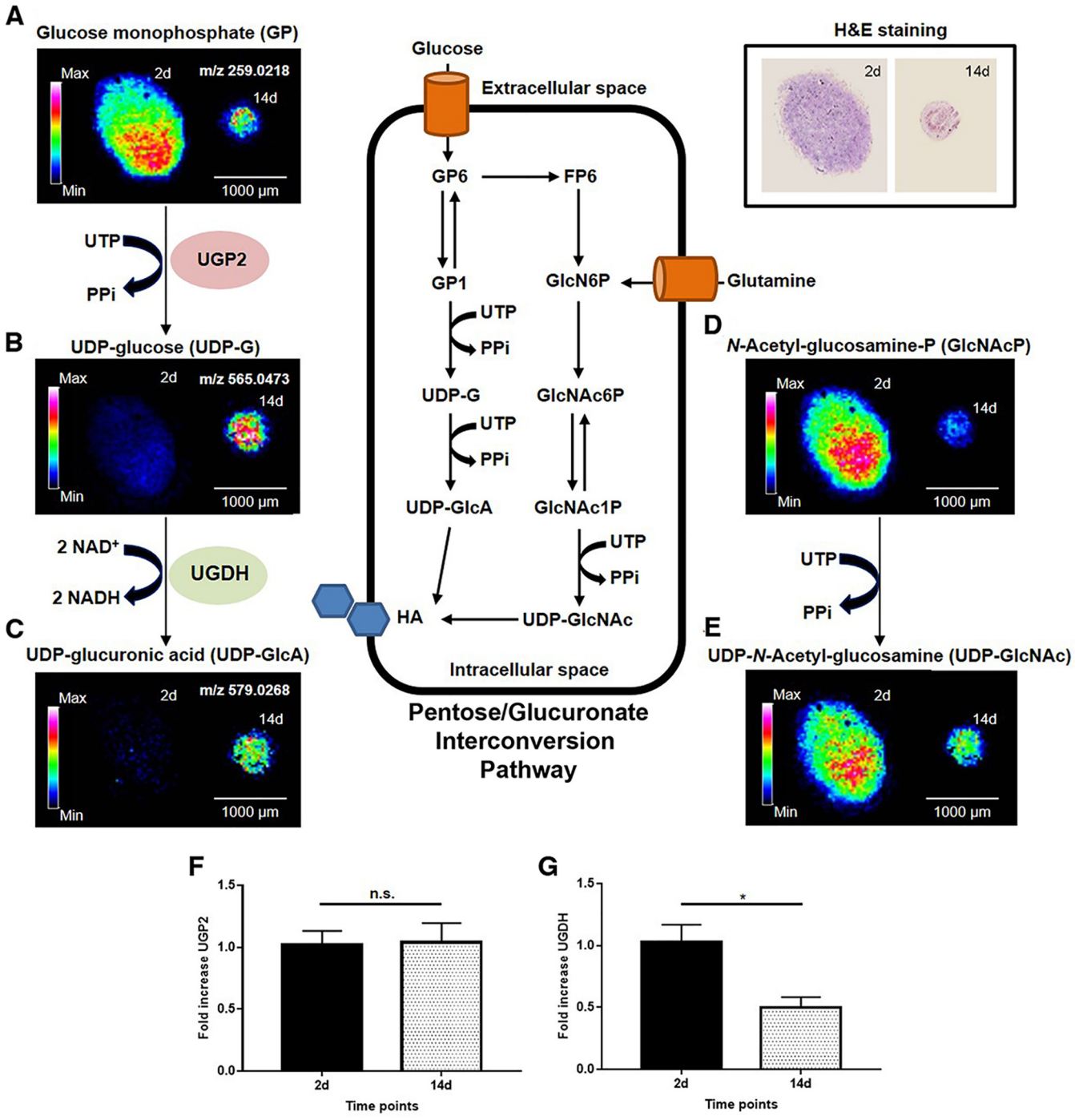

FIG. 5. **Spatial distribution and metabolic changes involved in the UDP-glucuronic acid interconversion pathway and amino sugar metabolism in OA hBMSCs.** *A–E*, MALDI-MSI images showing the abundance and spatial distribution of glucose monophosphate (*A*), UDP-glucose (*B*), UDP-glucuronic acid (*C*), *N*-Acetyl-glucosamine-phosphate (*D*) and UDP-*N*-Acetyl-glucosamine (*E*) in OA micromasses at days 2 (left) and 14 (right) of chondrogenesis. *F*, *G*, Gene expression levels determined by qRT-PCR of UTP-glucose-1-phosphate uridylyltransferase (*F*) and UDP-glucose 6-dehydrogenase (*G*). In (A-E), data were normalized by root means square. In (*F–G*), data are expressed as mean ± SEM of 5 independent experiments. * p value < 0.05, n.s. not significant.

cleotides, 6 sugar phosphates, 5 phosphatidic acid (PA)-related metabolites, 3 inositol-related metabolites, 2 fatty acids, and 1 sugar nucleotide. Finally, 15 phospholipid species were also identified. The statistical analysis of these data revealed that undifferentiated hBMSCs from OA patients contained higher levels of sugars such as inositol phosphate, glucose monophosphate, fructose 1,6-bisphosphate (Fru-1,6-P2), and ribose 5-phosphate compared with control cells (supplemental Fig. S6).

Finally, we carried out a metabolite set enrichment analysis (MSEA) to identify which pathways were affected at this early chondrogenic differentiation stage. Our results revealed 20 enriched pathways (supplemental Fig. S7), of which 4 were significantly up-regulated in OA (p value <0.02): the pentose phosphate pathway (PPP), Warbur effect, lactose synthesis and gluconeogenesis. Next, we performed a metabolic pathway analysis using MetaboAnalyst to characterize the functional role of these metabolites and to estimate the node importance within the pathways. According to this analysis, we confirmed the finding that purine metabolism and the PPP were significantly altered (p value < 0.025) in OA hBMSCs compared with controls at day 2 (supplemental Fig. S7, supplemental Table S11). The intensity and spatial distribution of several metabolites involved in the PPP in OA and control micromass sections obtained at day 2 were examined using FlexImaging software (supplemental Fig. S8). Among these metabolites, ribose-5-phosphate and ribose 1,5-bisphosphate were differentially distributed across the micromass sections, with a relative higher intensity in the peripheral cells of the control micromasses. On the contrary, both metabolites were primarily detected in the cells located in the core of OA micromasses, suggesting a higher degree of proliferation in this area.

DISCUSSION

Drugs stimulating the *in vivo* induction of chondrogenesis in MSCs have been suggested as a promising therapeutic approach for osteoarthritis treatment (36), as they may contribute to overcome the restricted regenerative capacity of articular cartilage. To provide novel targets for the development of DMOADs, proteomic and metabolomic approaches have been combined to identify alterations in metabolic pathways underlying the early phases of cartilage formation in an *in vitro* 3D model of osteoarthritic hBMSCs and healthy controls. Initially, the chondrogenic differentiation of control and OA hBMSCs in our model was evaluated using IHC assays. Although a higher expression of GAGs such as CH_6S and KS was found in both healthy and diseased cellular models at day 14 of chondrogenesis, OA hBMSCs did also show a higher hypertrophic/fibrotic phenotype at the differentiated chondrogenic stage. MSC hypertrophy is characterized by an increase in cell volume, expression of collagen type X, matrix metalloproteinases and alkaline phosphatase activity (37). In addition, MSCs with hypertrophic phenotype express and produce collagen type I preferentially over collagen type II (38), which is indicative of fibrocartilage instead of hyaline cartilage formation. Therefore, promoting chondrogenic differentiation while preventing hypertrophy of chondrogenic MSCs is essential for the application of MSCs in strategies for cartilage regeneration. Accordingly, the observed differences support the hipothesis of molecular alterations underlying the MSCs differentiation in OA.

To elucidate these derangements, a SILAC strategy was carried out to quantitatively describe the intracellular protein profiles of OA hBMSCs undergoing chondrogenic differentiation. Fourty-three proteins were altered with statistical significance between two early steps of chondrogenesis, day 2 and day 14 (Table I). From this subset of proteins, the largest functional group included those involved in metabolic processes, an essential topic to understand chondrogenesis, cartilage physiology and pathophysiology (39). All these proteins were increased at day 14 of chondrogenesis, except for UGDH. Moreover, most of the modulated proteins were involved in the glycolysis pathway, indicating an enhanced glycolytic activity induced by chondrogenic differentiation. This is consistent with the glycolytic nature of cartilage and agrees with previously reported higher rates of glycolysis following chondrogenic differentiation, when compared with proliferative MSCs (40, 41). All these data provide support to the key role of metabolic changes, particularly an enhancement of the glycolytic pathway, in the regulation of hBMSCs chondrogenesis. Together with our previous published data about proteomic changes of healthy hBMSCs undergoing this process, it can be concluded that a shift toward glycolysis is a common metabolic feature in the chondrogenesis of both OA and control hBMSCs. This also points out that early-differentiated cells mainly rely on glycolysis as an energy source.

Metabolomic analyses have recently been employed to investigate the effects of different culture conditions on MSCs metabolism during adipogenic and osteogenic differentiation (42–44). For instance, the addition of L-carnitine during the adipogenic differentiation of BMSCs decreased the levels of many saturated and unsaturated long-chain fatty acids, as well as the production of metabolites involved in glycolysis, gluconeogenesis, and pyruvate metabolism pathways (45). Based on the culture oxygen levels, Muñoz *et al.* described differences in glutaminolysis, the tricarboxylic acid cycle, and the malate-aspartate shuttle during the osteogenic differentiation of hBMSCs (43). Finally, the use of metabolic profiles as markers of MSCs chondrogenic differentiation has been proposed (19).

In the present work, we have applied for the first time the MALDI-FT-ICR-MSI technology to characterize and localize metabolic changes in control and OA hBMSCs during the early stages of chondrogenesis. This metabolomic analysis provided key findings, including the identification of 35 metabolites significantly altered in the differentiation of OA hBMSCs when compared with controls. These metabolites, in combination with the 43 proteins differentially regulated in OA chondrogenesis, were mapped into several interconnected pathways (supplemental Fig. S9). Remarkably, the levels of metabolites involved in the synthesis of UDP-glucuronic synthesis were consistently altered in OA cells (Fig. 5). We observed at day 14 an accumulation of the precursor UDP-glucose in OA cells compared with controls. A feasible reason for this accumulation might be the down-regulation of the

UGDH enzyme that we also detect in this work, in this case by proteomics and gene expression analyses. UGDH is required for the conversion of UDP-glucose into UDP-glucuronic acid, thus being directly involved in the synthesis of cartilage GAGs and PGs (46). Interestingly, an increase of UGDH has been described during aging and is linked with HA accumulation and signaling alterations (47, 48). Other investigations have also demonstrated that the regulation of UGDH expression levels promotes a marked increase of GAGs and enhances chondrogenesis in micromass cultures *in vitro* (49). In cartilage, UGDH protein expression is decreased in the osteoarthritic tissue compared with normal (50). The down-regulation of UGDH that we report herein may negatively affect the synthesis of UDP-glucuronic acid, and consequently alter the production of ECM PGs and GAGs that is required for the proper functionality of cartilage. Moreover, the UDP-glucuronic acid can be decarboxylated to UDP-xylose, which is critical for the linking of GAGs to proteoglycan core proteins (51).

Additionally, this work evidences the alteration of the amino sugar metabolism (hexosamine pathway) in the chondrogenesis of OA hBMSCs compared with controls. Glucosamine (GlcN) is an important amino sugar present in the articular cartilage ECM, and a precursor for GAGs and PG synthesis. Several previous studies have explored the effects of GlcN and its derivates, such as GlcNAc, on cartilage repair. These studies demonstrated the ability of these molecules to enhance the biosynthesis of relevant cartilage PGs and to prevent inflammation by inhibiting the activity of pro-inflammatory mediators (52–54). Moreover, GlcN was shown to promote chondrogenesis and stimulate GAGs synthesis through the increase of transforming growth factor β1 gene expression (55). Additionally, a modified polyethylene glycol hydrogels with GlcN has recently been reported to enhance the chondrogenesis of hBMSCs with low fibrosis and expression of hypertrophic cartilage markers (56). In our study, the levels of GlcNAc and UDP-GlcNAc were significantly decreased in OA hBMSCs after 14 days of differentiation. The reduction of these two intermediates may impair HA, PGs and GAGs production. Altogether, these results strongly suggest that the UDP-glucuronic acid synthesis pathway could serve as a therapeutic target for enhancing cartilage ECM formation in OA.

Finally, we evaluated the molecular changes undergoing control and OA hBMSCs at day 2 of chondrogenesis. Our metabolomic analysis demonstrated that ribose-5-phosphate and ribose-1,5-bisphosphate are significantly increased in OA, pointing to an enhanced activity of the PPP compared with controls. The PPP produces ribose-5-phosphate for the *novo* nucleotide synthesis (57). Our results suggest that OA hBMSCs preferentially use the oxidative branch of this pathway to acquire the ribose-5-phosphate that is essential for cell proliferation through DNA and RNA synthesis. This might suggest that OA hBMSCs at day 2 could maintain a proliferative stage (especially those cells located at the micromass core) compared with controls, which in turn could initiate an early chondrogenic differentiation. Altogether, these metabolic alterations detected at the undifferentiated state might indicate an earlier upstream dysregulation in the chondrogenic differentiation of OA cells.

In conclusion, our findings reveal a critical role of specific metabolic processes as key regulators at the early onset of chondrogenic differentiation. Exploring further these pathways is expected to improve understanding on the metabolic regulation of chondrogenesis in normal and diseased contexts. Specifically, the alterations in the UDP-glucuronic acid synthesis pathway reported herein provide novel molecular targets that could be investigated for future therapeutic development in diseases affecting the cartilage such as OA.

Acknowledgments—We thank the Pathology Service from the Orthopaedics Department of the CHU A Coruña for providing bone marrow samples, to Tamara Hermida for hBMSCs isolation and characterization, and to Noa Goyanes for obtaining the micromass sections. We would also like to thank Maria Eugenia Vázquez Mosquera for helping with the qRT-PCR data analysis and IHC quantifications.

DATA AVAILABILITY

The mass spectrometry proteomics data have been deposited to the ProteomeXchange Consortium via the PRIDE partner repository (https://www.ebi.ac.uk/pride/archive/projects/PXD012879) with the dataset identifier PXD012879 and the project name of MSCs OA SILAC Mass spectrometry imaging.

* This work has been funded by Fondo Investigación Sanitaria-Spain (grant numbers PI14/01707, PI16/02124, PI17/00404, DTS17/00200, CIBER-CB06/01/0040 and RETIC-RIER-RD12/0009/0018), a part of the National Plan for Scientific Program Development and Technological Innovation 2013–2016, funded by the ISCIII-General Subdirection of Assessment and Promotion of Research - European Regional Development Fund (FEDER) "A way of making Europe." The Proteomics Unit of GIR belongs to ProteoRed, PRB2- ISCIII (grant number PT17/0019/0014). B.R. is supported by Xunta de Galicia (IN606B-2016/004). The research was partially performed within the M4I research program, financially supported by the Dutch Province of Limburg as part of the "LINK" program. The authors declare that they have no conflicts of interest with the contents of this article.

S This article contains supplemental material.

** To whom correspondence may be addressed: INIBIC-Complejo Hospitalario Universitario A Coruña, C/As Xubias, 84; 15006 A Coruña, Spain. Tel.: 34-981-176399; Fax: 34-981-176398; E-mail: fblagar@sergas.es.

‡‡ To whom correspondence may be addressed. E-mail: valentina.calamia@sergas.es.

Author contributions: B.R., C.R.-R., and F.J.B. designed research; B.R., B.C.-P., G.E., P.F.-P., M.R.L.P., R.M.A.H., and V.C. performed research; B.R., B.C.-P., G.E., P.F.-P., M.R.L.P., C.R.-R., R.M.A.H., V.C., and F.J.B. analyzed data; B.R., B.C.-P., G.E., P.F.-P., M.R.L.P., C.R.-R., R.M.A.H., V.C., and F.J.B. wrote the paper; B.C.-P., G.E., C.R.-R., R.M.A.H., and F.J.B. contributed new reagents/analytic tools.

REFERENCES

1. Oldershaw, R. A. (2012) Cell sources for the regeneration of articular cartilage: the past, the horizon and the future. *Int. J. Exp. Pathol.* **93,** 389–400
2. Poole, A. R. (2012) Osteoarthritis as a whole joint disease. *HSS J.* **8,** 4–6
3. Alsalameh, S., Amin, R., Gemba, T., and Lotz, M. (2004) Identification of mesenchymal progenitor cells in normal and osteoarthritic human articular cartilage. *Arthritis Rheum.* **50,** 1522–1532
4. Hermida-Gómez, T., Fuentes-Boquete, I., Gimeno-Longas, M. J., Muiños-López, E., Díaz-Prado, S., de Toro, F. J., and Blanco, F. J. (2011) Quantification of cells expressing mesenchymal stem cell markers in healthy and osteoarthritic synovial membranes. *J. Rheumatol.* **38,** 339–349
5. Sekiya, I., Ojima, M., Suzuki, S., Yamaga, M., Horie, M., Koga, H., Tsuji, K., Miyaguchi, K., Ogishima, S., Tanaka, H., and Muneta, T. (2012) Human mesenchymal stem cells in synovial fluid increase in the knee with degenerated cartilage and osteoarthritis. *J. Orthop. Res.* **30,** 943–949
6. Matsukura, Y., Muneta, T., Tsuji, K., Koga, H., and Sekiya, I. (2014) Mesenchymal stem cells in synovial fluid increase after meniscus injury. *Clin. Orthop. Relat. Res.* **472,** 1357–1364
7. Blanco, F. J., and Ruiz-Romero, C. (2013) New targets for disease modifying osteoarthritis drugs: chondrogenesis and Runx1. *Ann. Rheum. Dis.* **72,** 631–634
8. Deshmukh, V., Hu, H., Barroga, C., Bossard, C., Kc, S., Dellamary, L., Stewart, J., Chiu, K., Ibanez, M., Pedraza, M., Seo, T., Do, L., Cho, S., Cahiwat, J., Tam, B., Tambiah, J. R. S., Hood, J., Lane, N. E., and Yazici, Y. (2018) A small-molecule inhibitor of the Wnt pathway (SM04690) as a potential disease modifying agent for the treatment of osteoarthritis of the knee. *Osteoarthritis Cartilage* **26,** 18–27
9. Jeon, Y. J., Kim, J., Cho, J. H., Chung, H. M., and Chae, J. I. (2016) Comparative Analysis of Human Mesenchymal Stem Cells Derived From Bone Marrow, Placenta, and Adipose Tissue as Sources of Cell Therapy. *J. Cell. Biochem.* **117,** 1112–1125
10. Henrionnet, C., Gillet, P., Mainard, D., Vincourt, J. B., and Pinzano, A. (2017) Label-free relative quantification of secreted proteins as a non-invasive method for the quality control of chondrogenesis in bioengineered substitutes for cartilage repair. *J. Tissue Eng. Regen. Med.* **12,** e1757–e1766
11. Peffers, M. J., Collins, J., Loughlin, J., Proctor, C., and Clegg, P. D. (2016) A proteomic analysis of chondrogenic, osteogenic and tenogenic constructs from ageing mesenchymal stem cells. *Stem Cell Res. Ther.* **7,** 133
12. Collier, T. S., Sarkar, P., Franck, W. L., Rao, B. M., Dean, R. A., and Muddiman, D. C. (2010) Direct comparison of stable isotope labeling by amino acids in cell culture and spectral counting for quantitative proteomics. *Anal. Chem.* **82,** 8696–8702
13. Li, Z., Adams, R. M., Chourey, K., Hurst, G. B., Hettich, R. L., and Pan, C. (2012) Systematic comparison of label-free, metabolic labeling, and isobaric chemical labeling for quantitative proteomics on LTQ Orbitrap Velos. *J. Proteome Res.* **11,** 1582–1590
14. Bantscheff, M., Schirle, M., Sweetman, G., Rick, J., and Kuster, B. (2007) Quantitative mass spectrometry in proteomics: a critical review. *Anal. Bioanal. Chem.* **389,** 1017–1031
15. Chen, X., Wei, S., Ji, Y., Guo, X., and Yang, F. (2015) Quantitative proteomics using SILAC: Principles, applications, and developments. *Proteomics* **15,** 3175–3192
16. Sury, M. D., Chen, J. X., and Selbach, M. (2010) The SILAC fly allows for accurate protein quantification in vivo. *Mol. Cell. Proteomics* **9,** 2173–2183
17. Rocha, B., Calamia, V., Mateos, J., Fernández-Puente, P., Blanco, F. J., and Ruiz-Romero, C. (2012) Metabolic labeling of human bone marrow mesenchymal stem cells for the quantitative analysis of their chondrogenic differentiation. *J. Proteome Res.* **11,** 5350–5361
18. Kwon, H. J., and Ohmiya, Y. (2013) Metabolomic analysis of differential changes in metabolites during ATP oscillations in chondrogenesis. *Biomed. Res. Int.* **2013,** 213972
19. Jang, M. Y., Chun, S. I., Mun, C. W., Hong, K. S., and Shin, J. W. (2013) Evaluation of metabolomic changes as a biomarker of chondrogenic differentiation in 3D-cultured human mesenchymal stem cells using proton (1H) nuclear magnetic resonance spectroscopy. *PLoS ONE* **8,** e78325
20. Rocha, B., Cillero-Pastor, B., Eijkel, G., Bruinen, A. L., Ruiz-Romero, C., Heeren, R. M., and Blanco, F. J. (2015) Characterization of lipidic markers of chondrogenic differentiation using mass spectrometry imaging. *Proteomics* **15,** 702–713
21. Altman, R., Asch, E., Bloch, D., Bole, G., Borenstein, D., Brandt, K., Christy, W., Cooke, T. D., Greenwald, R., and Hochberg, M. (1986) Development of criteria for the classification and reporting of osteoarthritis. Classification of osteoarthritis of the knee. Diagnostic and Therapeutic Criteria Committee of the American Rheumatism Association. *Arthritis Rheum.* **29,** 1039–1049
22. Rocha, B., Calamia, V., Casas, V., Carrascal, M., Blanco, F. J., and Ruiz-Romero, C. (2014) Secretome analysis of human mesenchymal stem cells undergoing chondrogenic differentiation. *J. Proteome Res.* **13,** 1045–1054
23. Cicione, C., Díaz-Prado, S., Muiños-López, E., Hermida-Gómez, T., and Blanco, F. J. (2010) Molecular profile and cellular characterization of human bone marrow mesenchymal stem cells: donor influence on chondrogenesis. *Differentiation* **80,** 155–165
24. Cicione, C., Muiños-López, E., Hermida-Gómez, T., Fuentes-Boquete, I., Díaz-Prado, S., and Blanco, F. J. (2013) Effects of severe hypoxia on bone marrow mesenchymal stem cells differentiation potential. *Stem Cells Int.* **2013,** 232896
25. Cicione, C., Muiños-López, E., Hermida-Gómez, T., Fuentes-Boquete, I., Díaz-Prado, S., and Blanco, F. J. (2015) Alternative protocols to induce chondrogenic differentiation: transforming growth factor-β superfamily. *Cell Tissue Bank* **16,** 195–207
26. Eijkel, G. B., Kaletas, B., Van der Wiel, I. M., Kros, J. M., Luinder, T. M., and Heeren, R. M. A. (2009) Correlating MALDI and SIMS imaging mass spectrometric datasets of biological tissue surfaces. *Surf. Interface* **41,** 675–685
27. Wishart, D. S., Jewison, T., Guo, A. C., Wilson, M., Knox, C., Liu, Y., Djoumbou, Y., Mandal, R., Aziat, F., Dong, E., Bouatra, S., Sinelnikov, I., Arndt, D., Xia, J., Liu, P., Yallou, F., Bjorndahl, T., Perez-Pineiro, R., Eisner, R., Allen, F., Neveu, V., Greiner, R., and Scalbert, A. (2013) HMDB 3.0–The Human Metabolome Database in 2013. *Nucleic Acids Res.* **41,** D801–D807
28. Smith, C. A., O'Maille, G., Want, E. J., Qin, C., Trauger, S. A., Brandon, T. R., Custodio, D. E., Abagyan, R., and Siuzdak, G. (2005) METLIN: a metabolite mass spectral database. *Ther. Drug Monit.* **27,** 747–751
29. Fahy, E., Sud, M., Cotter, D., and Subramaniam, S. (2007) LIPID MAPS online tools for lipid research. *Nucleic Acids Res.* **35,** W606–W612
30. Chong, J., Soufan, O., Li, C., Caraus, I., Li, S., Bourque, G., Wishart, D. S., and Xia, J. (2018) MetaboAnalyst 4.0: towards more transparent and integrative metabolomics analysis. *Nucleic Acids Res.* **46,** W486–W494
31. Kanehisa, M., Goto, S., Sato, Y., Kawashima, M., Furumichi, M., and Tanabe, M. (2014) Data, information, knowledge and principle: back to metabolism in KEGG. *Nucleic Acids Res.* **42,** D199–D205
32. Jewison, T., Su, Y., Disfany, F. M., Liang, Y., Knox, C., Maciejewski, A., Poelzer, J., Huynh, J., Zhou, Y., Arndt, D., Djoumbou, Y., Liu, Y., Deng, L., Guo, A. C., Han, B., Pon, A., Wilson, M., Rafatnia, S., Liu, P., and Wishart, D. S. (2014) SMPDB 2.0: big improvements to the Small Molecule Pathway Database. *Nucleic Acids Res.* **42,** D478–D484
33. Wilusz, R. E., Sanchez-Adams, J., and Guilak, F. (2014) The structure and function of the pericellular matrix of articular cartilage. *Matrix Biol.* **39,** 25–32
34. Luo, Y., Sinkeviciute, D., He, Y., Karsdal, M., Henrotin, Y., Mobasheri, A., Önnerfjord, P., and Bay-Jensen, A. (2017) The minor collagens in articular cartilage. *Protein Cell* **8,** 560–572
35. Hasegawa, M., Yoshida, T., and Sudo, A. (2018) Role of tenascin-C in articular cartilage. *Mod. Rheumatol.* **28,** 215–220
36. Roubille, C., Pelletier, J. P., and Martel-Pelletier, J. (2013) New and emerging treatments for osteoarthritis management: will the dream come true with personalized medicine? *Expert Opin. Pharmacother.* **14,** 2059–2077
37. Studer, D., Millan, C., Öztürk, E., Maniura-Weber, K., and Zenobi-Wong, M. (2012) Molecular and biophysical mechanisms regulating hypertrophic differentiation in chondrocytes and mesenchymal stem cells. *Eur. Cell Mater.* **24**, 118–135; discussion 135
38. Scotti, C., Tonnarelli, B., Papadimitropoulos, A., Scherberich, A., Schaeren, S., Schauerte, A., Lopez-Rios, J., Zeller, R., Barbero, A., and Martin, I. (2010) Recapitulation of endochondral bone formation using human adult

mesenchymal stem cells as a paradigm for developmental engineering. *Proc. Natl. Acad. Sci. U.S.A.* **107,** 7251–7256
39. Mobasheri, A., Vannucci, S. J., Bondy, C. A., Carter, S. D., Innes, J. F., Arteaga, M. F., Trujillo, E., Ferraz, I., Shakibaei, M., and Martín-Vasallo, P. (2002) Glucose transport and metabolism in chondrocytes: a key to understanding chondrogenesis, skeletal development and cartilage degradation in osteoarthritis. *Histol. Histopathol.* **17,** 1239–1267
40. Wang, D. W., Fermor, B., Gimble, J. M., Awad, H. A., and Guilak, F. (2005) Influence of oxygen on the proliferation and metabolism of adipose derived adult stem cells. *J. Cell. Physiol.* **204,** 184–191
41. Meleshina, A. V., Dudenkova, V. V., Bystrova, A. S., Kuznetsova, D. S., Shirmanova, M. V., and Zagaynova, E. V. (2017) Two-photon FLIM of NAD(P)H and FAD in mesenchymal stem cells undergoing either osteogenic or chondrogenic differentiation. *Stem Cell Res. Ther.* **8,** 15
42. Klontzas, M. E., Vernardis, S. I., Heliotis, M., Tsiridis, E., and Mantalaris, A. (2017) Metabolomics analysis of the osteogenic differentiation of umbilical cord blood mesenchymal stem cells reveals differential sensitivity to osteogenic agents. *Stem Cells Dev.* **26,** 723–733
43. Muñoz, N., Kim, J., Liu, Y., Logan, T. M., and Ma, T. (2014) Gas chromatography-mass spectrometry analysis of human mesenchymal stem cell metabolism during proliferation and osteogenic differentiation under different oxygen tensions. *J. Biotechnol.* **169,** 95–102
44. Tan, J., Wang, Y., Wang, S., Zhang, N., Wu, S., Yuan, Z., and Zhu, X. (2017) Untargeted metabolomics analysis of adipogenic transformation in OP9-DL1 cells using liquid chromatography-mass spectrometry: Implications for thymic adipogenesis. *Cell Biol. Int.* **41,** 447–456
45. Fujisawa, K., Takami, T., Fukui, Y., Quintanilha, L. F., Matsumoto, T., Yamamoto, N., and Sakaida, I. (2017) Evaluating effects of L-carnitine on human bone-marrow-derived mesenchymal stem cells. *Cell Tissue Res.* **368,** 301–310
46. Egger, S., Chaikuad, A., Kavanagh, K. L., Oppermann, U., and Nidetzky, B. (2010) UDP-glucose dehydrogenase: structure and function of a potential drug target. *Biochem. Soc. Trans.* **38,** 1378–1385
47. Simpson, R. M., Wells, A., Thomas, D., Stephens, P., Steadman, R., and Phillips, A. (2010) Aging fibroblasts resist phenotypic maturation because of impaired hyaluronan-dependent CD44/epidermal growth factor receptor signaling. *Am. J. Pathol.* **176,** 1215–1228
48. Cargill, R., Kohama, S. G., Struve, J., Su, W., Banine, F., Witkowski, E., Back, S. A., and Sherman, L. S. (2012) Astrocytes in aged nonhuman primate brain gray matter synthesize excess hyaluronan. *Neurobiol. Aging* **33,** 830.e813–e824
49. Clarkin, C. E., Allen, S., Kuiper, N. J., Wheeler, B. T., Wheeler-Jones, C. P., and Pitsillides, A. A. (2011) Regulation of UDP-glucose dehydrogenase is sufficient to modulate hyaluronan production and release, control sulfated GAG synthesis, and promote chondrogenesis. *J. Cell. Physiol.* **226,** 749–761
50. Wen, Y., Li, J., Wang, L., Tie, K., Magdalou, J., Chen, L., and Wang, H. (2014) UDP-glucose dehydrogenase modulates proteoglycan synthesis in articular chondrocytes: its possible involvement and regulation in osteoarthritis. *Arthritis Res. Ther.* **16,** 484
51. Vigetti, D., Karousou, E., Viola, M., Deleonibus, S., De Luca, G., and Passi, A. (2014) Hyaluronan: biosynthesis and signaling. *Biochim. Biophys. Acta* **1840,** 2452–2459
52. Varghese, S., Theprungsirikul, P., Sahani, S., Hwang, N., Yarema, K. J., and Elisseeff, J. H. (2007) Glucosamine modulates chondrocyte proliferation, matrix synthesis, and gene expression. *Osteoarthritis Cartilage* **15,** 59–68
53. Shikhman, A. R., Amiel, D., D'Lima, D., Hwang, S. B., Hu, C., Xu, A., Hashimoto, S., Kobayashi, K., Sasho, T., and Lotz, M. K. (2005) Chondroprotective activity of N-acetylglucosamine in rabbits with experimental osteoarthritis. *Ann. Rheum. Dis.* **64,** 89–94
54. Shikhman, A. R., Kuhn, K., Alaaeddine, N., and Lotz, M. (2001) N-acetylglucosamine prevents IL-1 beta-mediated activation of human chondrocytes. *J. Immunol.* **166,** 5155–5160
55. Hwang, N. S., Varghese, S., Theprungsirikul, P., Canver, A., and Elisseeff, J. (2006) Enhanced chondrogenic differentiation of murine embryonic stem cells in hydrogels with glucosamine. *Biomaterials* **27,** 6015–6023
56. Yao, H., Xue, J., Wang, Q., Xie, R., Li, W., Liu, S., Cai, J., Qin, D., Wang, D. A., and Ren, L. (2017) Glucosamine-modified polyethylene glycol hydrogel-mediated chondrogenic differentiation of human mesenchymal stem cells. *Mater. Sci. Eng. C Mater. Biol. Appl.* **79,** 661–670
57. Stincone, A., Prigione, A., Cramer, T., Wamelink, M. M., Campbell, K., Cheung, E., Olin-Sandoval, V., Grüning, N. M., Krüger, A., Tauqeer Alam, M., Keller, M. A., Breitenbach, M., Brindle, K. M., Rabinowitz, J. D., and Ralser, M. (2015) The return of metabolism: biochemistry and physiology of the pentose phosphate pathway. *Biol. Rev. Camb. Philos. Soc.* **90,** 927–963